Environ. Sci. Technol. **2010,** *44,* 8467–8472

Arsenite Oxidation by a Poorly Crystalline Manganese-Oxide. 2. Results from X-ray Absorption Spectroscopy and X-ray Diffraction

BRANDON J. LAFFERTY,* MATTHEW GINDER-VOGEL,† MENGQIANG ZHU, KENNETH J. T. LIVI,‡ AND DONALD L. SPARKS

Department of Plant and Soil Sciences, Delaware Environmental Institute, University of Delaware, 152 Townsend Hall, Newark, Delaware 19716, United States

Received June 14, 2010. Revised manuscript received September 23, 2010. Accepted October 1, 2010.

Arsenite (As^{III}) oxidation by manganese oxides (Mn-oxides) serves to detoxify and, under many conditions, immobilize arsenic (As) by forming arsenate (As^{V}). As^{III} oxidation by Mn^{IV}-oxides can be quite complex, involving many simultaneous forward reactions and subsequent back reactions. During As^{III} oxidation by Mn-oxides, a reduction in oxidation rate is often observed, which is attributed to Mn-oxide surface passivation. X-ray absorption spectroscopy (XAS) and X-ray diffraction (XRD) data show that Mn^{II} sorption on a poorly crystalline hexagonal birnessite (δ-MnO_2) is important in passivation early during reaction with As^{III}. Also, it appears that Mn^{III} in the δ-MnO_2 structure is formed by conproportionation of sorbed Mn^{II} and Mn^{IV} in the mineral structure. The content of Mn^{III} within the δ-MnO_2 structure appears to increase as the reaction proceeds. Binding of As^{V} to δ-MnO_2 also changes as Mn^{III} becomes more prominent in the δ-MnO_2 structure. The data presented indicate that As^{III} oxidation and As^{V} sorption by poorly crystalline δ-MnO_2 is greatly affected by Mn oxidation state in the δ-MnO_2 structure.

Introduction

Manganese-oxides (Mn-oxides) commonly occur as fine-grained particles or coatings in terrestrial and aquatic environments, usually exhibiting high reactivity due to their large surface area and negative charge (*1*). They tend to exhibit a high sorption capacity for metals and are among the most potent oxidants in terrestrial and aquatic environments (*1*). Thus, Mn-oxides can influence the environment much more than some other, more abundant minerals. Biological Mn^{II} oxidation proceeds much more rapidly than abiotic Mn^{II} oxidation, which has led to the conclusion that many Mn-oxides in the environment are formed by microorganisms (i.e., are biogenic) (*2*). Many biogenic Mn-oxides are phyllomanganates with structures similar to that of hexagonal birnessite and are highly reactive with respect to metal sorption and oxidation (*3*−*7*).

* Corresponding author phone: (302) 831-3219; fax: (302) 831-0605; e-mail: bjl@udel.edu.

† Current address: Calera Corporation, 14600 Winchester Blvd., Los Gatos, CA 95030.

‡ Current address: Departments of Earth and Planetary Sciences and Biology, The Johns Hopkins University, Baltimore, MD 21218.

Arsenic (As) is a toxic element commonly occurring in the environment via natural processes and anthropogenic activities. In soils and sediments, the toxicity and mobility of As are determined, to a great extent, by its speciation. Specifically, arsenite (As^{III}) is more toxic than arsenate (As^{V}) (*8*), and the sorption of As by oxide minerals can be heavily dependent on pH and its speciation (*9, 10*). Several Mn-oxides, including phyllomanganates, are able to oxidize As^{III} to As^{V} (*11*−*17*), and because As^{III} is more toxic than As^{V} this process can be important as an As detoxification pathway in the environment. Along with detoxifying As, As^{III} oxidation by Mn-oxides can alter As mobility, often making it less mobile (*9, 10*).

Mechanisms of As^{III} oxidation by Mn-oxides can be quite complex, involving several reactions simultaneously. For example, As^{III} oxidation by birnessite produces As^{V} and Mn^{II} as reaction products (*11, 15*−*19*). However, both As^{V} and Mn^{II} can be adsorbed by birnessite (*15, 19*). Also, a Mn^{III} intermediate can form during As^{III} oxidation by Mn-oxides (*11, 20*). A phenomenon commonly observed during the oxidation of As^{III} by birnessite is passivation of the mineral surface (*11, 14*−*17, 21, 22*). That is to say, as the reaction between birnessite and As^{III} proceeds, the rate of As^{III} oxidation decreases with time. There are two potential mechanisms for Mn-oxide passivation during As^{III} oxidation. Sorption of Mn^{II}, produced by reducing Mn^{IV} in the mineral structure, can also block reactive sites on the mineral surface (*15, 18, 21*). Also, the formation of Mn^{III} on Mn-oxide surfaces, which are considered to be less reactive than Mn^{IV} sites, can decrease As^{III} oxidation rate (*11, 20, 23*).

In a previous study, it was shown that sorption of As is not involved in δ-MnO_2 passivation during As^{III} oxidation (*18*). Also, Mn^{II} was shown to be the primary reduced product of As^{III} oxidation on pristine δ-MnO_2 (*18*). In this study, the speciation of As and Mn in the solid phase are investigated during As^{III} oxidation by δ-MnO_2. To achieve this, stirred-flow reactions are stopped after various reaction times (Figure S1) and reacted δ-MnO_2 is collected for analysis by spectroscopic, diffraction, and microscopic techniques. The goals of this study are to characterize As sorption, Mn^{II} sorption, and Mn^{III} formation on δ-MnO_2 as they change over time during As^{III} oxidation. This study also aims to clarify the passivation mechanism(s) of birnessite during As^{III} oxidation. It is important to understand the mechanism(s) responsible for birnessite passivation in nature in order to better predict Mn-oxide reactivity and contaminant mobility in natural systems.

Materials and Methods

δ-MnO_2 Synthesis and Characterization. δ-MnO_2, a poorly crystalline Mn-oxide mineral, was synthesized for the experiments presented in this work. The procedures used to synthesize δ-MnO_2 as well as a description of characterization procedures are included in the companion paper (*18*).

Stirred-Flow Experiments. As^{III} oxidation by δ-MnO_2 was investigated using the same stirred-flow protocol and reaction conditions described in the companion paper (*18*). In order to monitor changes occurring in the solid phase during As^{III} oxidation by δ-MnO_2, the reaction was stopped and the solid phase collected for analysis after 0.5, 4, 10, 24, and 48 h of reaction (Figure S1). During As^{III} oxidation by δ-MnO_2, As sorption is greatest at 0.5 h, while maximum As^{V} appears in the stirred-flow effluent at 4 h of reaction. The sample at 10 h is near the end of As sorption during As^{III} oxidation and also

10.1021/es102016c
Published on Web 10/26/2010

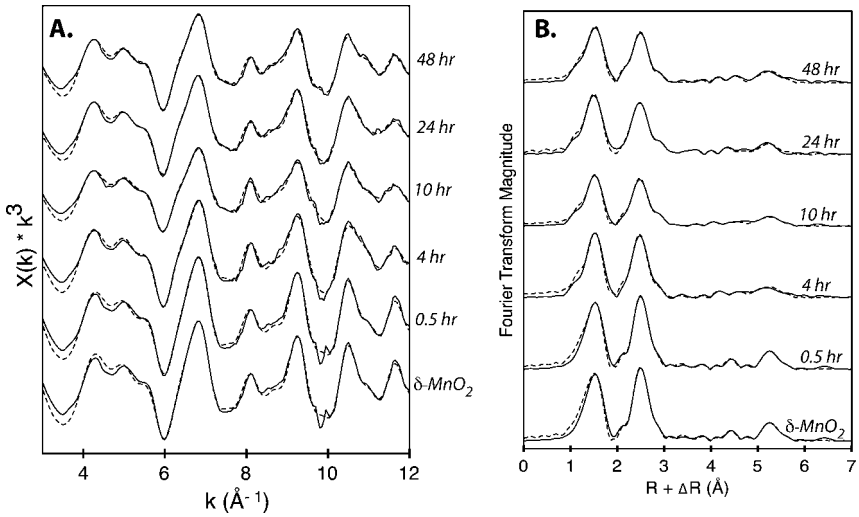

FIGURE 1. Manganese K-edge EXAFS (A) (6−10 Å^{-1}) and Fourier transformed EXAFS (B) of unreacted δ-MnO_2 and δ-MnO_2 (1.0 mg/L) reacted with As^{III} (100 μM) in a stirred-flow reactor for 0.5, 4, 10, 24, and 48 h. XAS data are presented as solid lines, and fits are presented as dashed lines (fit data provided in Table S1).

occurs early in the second phase of the reaction. The samples at 24 and 48 h are both during the less reactive phase of the reaction.

To stop the reaction, influent solution was removed, and the suspension in the reaction chamber was immediately filtered (0.22 μm) to remove any background electrolyte, Mn, and As not bound to δ-MnO_2. After filtration, some of the residual wet paste was immediately covered by Kapton tape and stored for less than 5 days prior to spectroscopic analysis. The remaining wet paste from each sample was refrigerated in sealed test tubes in the dark for less than 5 days for analysis by high resolution transmission electron microscopy (TEM) and synchrotron based X-ray diffraction (XRD). As^V sorption standards were prepared by reacting 100 μM As^V with 1 g/L δ-MnO_2 or Manganite (γ-MnOOH) for 24 h in the same background electrolyte used in stirred-flow reactions. Sorption standards were filtered, and the residual wet paste was immediately covered with Kapton tape and stored for less than 5 days for spectroscopic analysis.

Solid-Phase Characterization. High resolution transmission electron microscopic (HR-TEM), synchrotron X-ray based XRD, extended X-ray absorption fine structure (EXAFS) spectroscopic, and X-ray absorption near edge (XANES) spectroscopic analyses were performed on unreacted δ-MnO_2 as well as δ-MnO_2 reacted with 100 μM As^{III} for 0.5, 4, 10, 24, and 48 h (described previously). Detailed descriptions of sample collection, data collection, and processing of samples analyzed using these techniques can be found in the Supporting Information.

Results and Discussion

δ-MnO_2 Structure. The method used to synthesize δ-MnO_2 in this study produces a phyllomanganate composed of sheets of edge-sharing Mn^{IV} octahedra, and little order in vertical stacking arrangement (i.e., turbostratic) (*3, 4*). The Mn K-edge EXAFS spectra have three features between 4 and 6 Å^{-1} (Figure 1), which is common for EXAFS patterns of phyllomanganates (*24*). XRD analysis of the δ-MnO_2 synthesized for this study shows only two predominant peaks (37° and 66° 2θ (Cu Kα)) and a broad feature between them, also characteristic of turbostratic phyllomanganates (Figure 2) (*4, 25*). The absence of shoulders or splitting in the two predominant XRD peaks (37° and 66°, Figure 2) along with the presence of single peaks at 8.1 and 9.25 Å^{-1} in the Mn EXAFS pattern of pristine δ-MnO_2 (0 h, Figure 1A) confirms that δ-MnO_2 exhibits hexagonal symmetry rather than triclinic (*24−26*). Also, in the XRD pattern of unreacted δ-MnO_2, the absence of a dip at 45° (arrow in Figure 2) indicates very little $Mn^{II/III}$ sorbed in interlayers (at vacancy sites) (*4, 25*), and the absence of a shoulder at ~6.5 Å^{-1} in the Mn EXAFS agrees with this observation (δ-MnO_2, Figure 1A) (*6*). One can also conclude that little Mn^{III} is present within pristine δ-MnO_2 layers, due to the average oxidation state of the starting material (3.95) (*18*), as well as the sharp peak at 9.25 Å^{-1} in the Mn EXAFS (δ-MnO_2, Figure 1A) (*27*).

A characteristic of hexagonal symmetry in the octahedral layers of birnessite minerals (such as δ-MnO_2) is the presence of vacancy sites. Vacancy sites resulting from the absence of a positively charged Mn^{IV} atom in the Mn octahedral layer are negatively charged and tend to sorb cations readily (*28−31*). When edge sites are present in large amounts on phyllomanganates (which is the case for minerals with small particle sizes), they can be important reactive sites as well (*11, 14, 32, 33*). δ-MnO_2 used in this research consists of small crystalline domains surrounded by HR-TEM amorphous material (Figure S2). It is difficult to accurately determine the size of crystalline domains in δ-MnO_2 using HR-TEM micrographs because crystalline particles are surrounded by TEM-amorphous material making them difficult to delineate. However, it is reasonable to conclude that the small particle size of δ-MnO_2 used in this study leads to the presence of a significant amount of edge sites. Therefore, the δ-MnO_2 used here has two predominant reaction sites: vacancy sites within Mn octahedral layers, and edge sites at Mn octahedral layer edges.

Mn Sorption on δ-MnO_2 during As^{III} Oxidation. When As^{III} is oxidized by δ-MnO_2 under the conditions studied here, only Mn^{II} is produced initially (*18*). However, Mn^{II} produced by As^{III} reaction with Mn^{IV} in δ-MnO_2 can undergo a 'back reaction' by sorbing on the δ-MnO_2 surface (*15, 21*). Heavy metals tend to have a higher sorption affinity for vacancy sites compared to edge sites in hexagonal birnessite (*29*). Thus, in this system, we expect Mn^{II} to sorb primarily at δ-MnO_2 vacancy sites until they are filled (or nearly filled) followed by sorption at available δ-MnO_2 edges sites.

When Mn^{II} sorbs at layer vacancy sites in hexagonal birnessite, it tends to form triple corner-sharing complexes (*29*), in which Mn^{II} shares corners of its octahedral coordination shell with corners of Mn^{IV} octahedra surrounding vacancy sites in Mn octahedral layers (*25*). Mn^{III} octahedra can also form these triple corner-sharing complexes when sorbed at δ-MnO_2 vacancy sites. A dip at 45° in XRD patterns of turbostratic phyllomanganates has previously been attributed to an increase in corner-sharing $Mn^{II/III}$ at vacancy

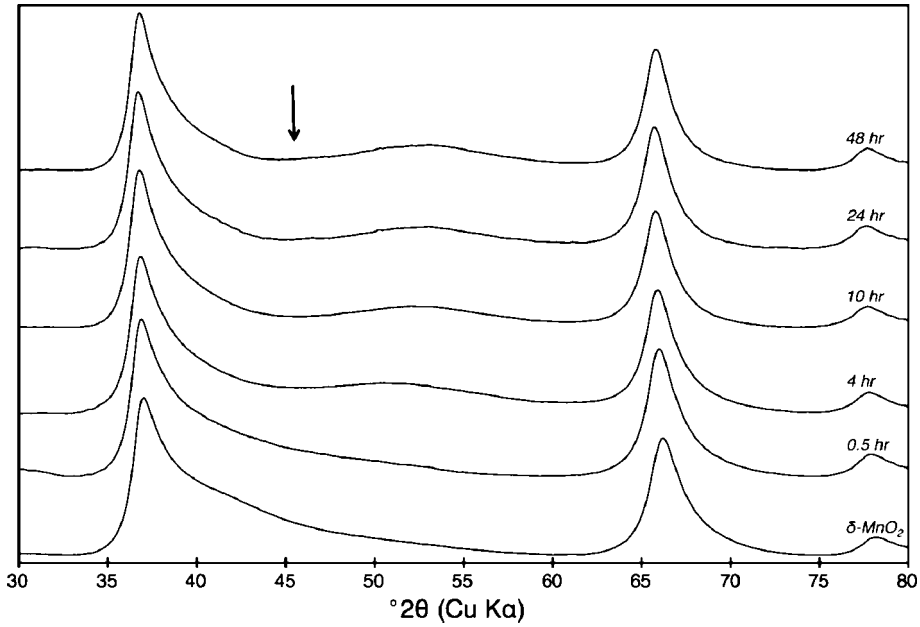

FIGURE 2. Synchrotron XRD patterns of unreacted δ-MnO_2 and δ-MnO_2 (1 mg/L) reacted with As^{III} (100 μM) in a stirred-flow reactor for 0.5, 4, 10, 24, and 48 h. Arrow indicates the position of the 'dip' at 45° that increases with reaction time.

sites (*4, 25*). When As^{III} is reacted with δ-MnO_2, this characteristic 'dip' in the XRD pattern of δ-MnO_2 appears at 45° (arrow in Figure 2). After 0.5 h, the dip at 45° is slight; however, it becomes more pronounced after 4 and 10 h. Beyond 10 h of As^{III} oxidation, the dip at 45° remains constant. Thus, XRD patterns of δ-MnO_2 confirm that as Mn^{II} is produced in the most reactive, early phase of As^{III} oxidation by δ-MnO_2 (*18*), it begins to sorb at vacancy sites immediately. Also, XRD data indicate that δ-MnO_2 vacancy sites are nearly fully occupied by triple corner-sharing $Mn^{II/III}$ within 4 h of reaction and are completely occupied between 4 and 10 h.

Mn sorbed at δ-MnO_2 vacancies in triple corner-sharing complexes can also be detected in Mn EXAFS data. Specifically, the shoulder at ~6.5 $Å^{-1}$ in EXAFS spectra (Figure 1A) and the peak at 2.9 Å ($R + \Delta R$) in the Fourier transformed data (Figure 1B) can be attributed to $Mn^{II/III}$ sorbed at vacancy sites in triple corner-sharing complexes (*6, 34, 35*). A slight increase is observed in the shoulder at ~6.5 $Å^{-1}$ in Mn EXAFS patterns during As^{III} oxidation (Figure 1A), and this trend can also be seen as an increase of the 2.9 Å ($R + \Delta R$) peak in the Fourier transformed data (Figure 1B). The 2.9 Å ($R + \Delta R$) peak of the Fourier transformed data exhibits its largest increase from 0 to 4 h, with a small increase between 4 and 10 h, and appears stable from 10 to 48 h (Figure 1B). Although difficult to discern, when examined closely, the trend in the 6.5 $Å^{-1}$ peak of the EXAFS data shows the same trend (Figure 1A). A decrease in the amplitude of first shell Mn−O and Mn−Mn peaks (1.53 and 2.49 Å ($R + \Delta R$), respectively) is also caused by $Mn^{II/III}$ sorption at vacancy sites (*6*), and both of these peaks decrease until 10 h of As^{III} oxidation by δ-MnO_2, providing further evidence that maximum $Mn^{II/III}$ sorption at vacancy sites is reached between 4 and 10 h (Figures 1B and Figure S3).

It can be concluded that the decrease in As^{V} sorption after ~3 h of reaction is due to increased competition between As^{V} and Mn^{II} for δ-MnO_2 edge sites (*18*). Both XRD and EXAFS analyses indicate vacancy sites are nearly fully occupied by $Mn^{II/III}$ after 4 h of As^{III} oxidation, which implies that beyond 4 h Mn^{II} produced during As^{III} oxidation increasingly competes with As for δ-MnO_2 edge sites. Also, XRD and EXAFS data show that δ-MnO_2 vacancy sites are fully occupied by Mn^{II} between 4 and 10 h of reaction, which is consistent with the first appearance of Mn^{II} in the stirred-flow effluent at 6.4 h (Figure S1).

Mn^{III} Formation during As^{III} Oxidation. Although initially δ-MnO_2 has very little Mn^{III} within its layers, the amount of Mn^{III} in its structure appears to increase as As^{III} oxidation proceeds. A broadening and decrease in peak height of the 9.25 $Å^{-1}$ peak in Mn EXAFS can be attributed to an increase in the Mn^{III} content within phyllomanganate layers (*24, 26, 36*). Mn^{III} content of up to ~20% in δ-MnO_2 has been observed by this change in the EXAFS spectra (with no splitting or leftward shift in the spectra reported until higher amounts of Mn^{III} are present) (*24, 26*). In the time-series data presented in Figure 1A, one can see the largest proportions of Mn^{III} in δ-MnO_2 layers occurring in the 10, 24, and 48 h samples, with a slight increase observed between 0.5 and 4 h as well as between 4 and 10 h. The broadening of the peak at 9.25 $Å^{-1}$ coincides with a decrease in the Mn−Mn multiple scattering peak in the Fourier transformed data at 5.2 Å ($R + \Delta R$) (Figure 1B). The Mn−Mn multiple scattering peak is not expected to be greatly affected by $Mn^{II/III}$ sorption at vacancy sites (*6*); however, it should be dramatically affected by the presence of Mn^{III} within octahedral layers (*5*). Therefore, we can conclude from Mn EXAFS data that Mn^{III} is not present in δ-MnO_2 layers in significant quantities before 0.5 h and is greatest from 10 to 48 h.

There are two possible mechanisms for formation of Mn^{III} during As^{III} oxidation by δ-MnO_2. First, Mn^{III} could be formed directly through Mn^{IV} oxidation of As^{III} (eq 1).

$$2(>Mn^{IV}{-}OH) + H_3As^{III}O_3(aq) + H_2O \rightarrow 2(>Mn^{III}{-}OH_2) + HAs^{V}O_4^{2-}(aq) + 2H^+ \quad (1)$$

Although this process does not occur in the first 10 h of reaction in this study (*18*), it has been reported previously in As^{III} oxidation by birnessite (*11, 20*). Another possible pathway for Mn^{III} formation is through conproportionation of Mn^{II} sorbed at Mn^{IV} sites on the δ-MnO_2 surface (eq 2).

$$>Mn^{IV}{-}OH + Mn^{II}(aq) + H_2O + H^+ \rightarrow 2(>Mn^{III}{-}OH_2) \quad (2)$$

This process has also been observed under reaction conditions similar to those used in this study (*37*). Although the mechanism of Mn^{III} formation within Mn octahedral sheets is not certain, EXAFS data indicate that as Mn^{III} is formed,

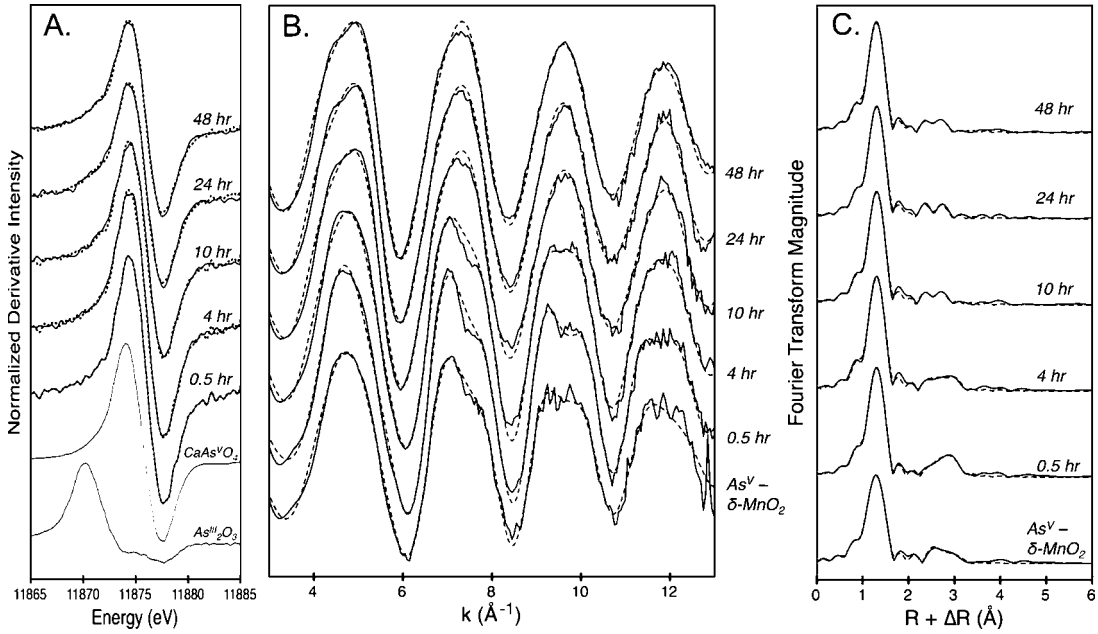

FIGURE 3. Arsenic K-edge derivative XANES (A), As K-edge EXAFS (B), and Fourier transformed EXAFS (C) of unreacted δ-MnO_2 and δ-MnO_2 (1 mg/L) reacted with As^{III} (100 μM) in a stirred-flow reactor for 0.5, 4, 10, 24, and 48 h. XAS data are presented as solid lines, and fits are presented as dashed lines (fit data provided in Table 1).

TABLE 1. Structural Parameters Derived from Least-Square Fits to Raw k^3-Weighted As-EXAFS Spectra for Sorption Standards and As^{III} Oxidation Samples Taken at 0.5, 4, 10, 24, and 48 h of Reaction

	As−O			As−Mn			As−Mn			As−Mn		
time, h	CN[a]	r[a]	σ^2 [a]	CN[a]	r[a]	σ^2 [a]	CN[a]	r[a]	σ^2 [a]	CN[a]	r[a]	σ^2 [a]
0.5	4.8(2)	1.70(0)	0.004(0)				1.3(2)	3.12(1)	0.005(2)	2.9(5)	3.42(1)	0.002(1)
4	3.8(3)	1.69(1)	0.003(1)				1.2(5)	3.13(4)	0.005(5)	1.4(6)	3.47(6)	0.009(3)
10	3.9(5)	1.69(1)	0.003(1)	0.3(2)	2.71(4)	0.006(3)	0.9(4)	3.20(3)	0.006(3)	0.4(5)	3.39(2)	0.006(3)
24	3.8(3)	1.69(1)	0.003(1)	0.4(2)	2.72(3)	0.006(3)	1.0(4)	3.23(3)	0.006(2)	0.4(5)	3.42(6)	0.006(3)
48	3.9(2)	1.69(1)	0.003(1)	0.21(3)	2.71(4)	0.006(2)	1.0(4)	3.19(3)	0.006(3)	0.6(4)	3.34(6)	0.006(4)
						As^{V}−Manganite						
	4.0(1)	1.69(1)	0.004(1)	0.1(1)	2.78(6)	0.006(3)	0.6(4)	3.35(1)	0.004(2)			
						As^{V}−δ-MnO_2						
	3.9(2)	1.70(1)	0.004(1)				0.9(5)	3.13(2)	0.003(2)	0.3(3)	3.48(4)	0.002(1)

[a] Coordination number (CN), interatomic distance (r), and Debye−Waller factor (σ^2) were obtained by fitting data with theoretical phase and amplitude functions. Estimated errors at 95% confidence interval from the least-squares fit are given in parentheses.

at least some is arranged in edge-sharing complexes on δ-MnO_2 edge sites (i.e., as part of the mineral structure) or around vacancy sites in octahedral layers of δ-MnO_2. Although its value is associated with rather large error, the trend in the fraction of Mn sites occupied in the δ-MnO_2 structure (f_{occ} from Mn EXAFS fitting) indicates that some Mn^{III} formed during As^{III} oxidation could enter into δ-MnO_2 vacancy sites (Table S1) (*36*).

As Speciation and Binding Mechanisms during As^{III} Oxidation. As K-edge XANES first derivative spectra show only As^{V} associated with δ-MnO_2 during As^{III} oxidation (Figure 3A). Shell-by-shell fits of the As EXAFS spectra indicate a first shell As−O distance of 1.7 Å exclusively (Table 1). An As−O bond distance of 1.7 Å is consistent with previously observed As^{V} bound to phyllomanganates (*14, 32*) and similar to As^{V} bound to Fe-oxides (*38, 39*). Previous studies have also found that during As^{III} oxidation by birnessite, As is bound to the solid phase only as As^{V} with no evidence of As^{III} (*11, 14*).

As K-edge EXAFS spectra exhibit a single major frequency (Figure 3B) which is due to the presence of four oxygen atoms surrounding As in tetrahedral coordination (*32*). This major frequency produces the predominant feature in the Fourier transformed data, an As−O peak at 1.3 Å ($R + \Delta R$) (Figure 3C). In addition to the As−O shell, several As−Mn shells occur between 2.2 and 3.2 Å ($R + \Delta R$) (Figure 3C). When As^{V} is reacted with δ-MnO_2 (sorption standard), two As−Mn distances are present (Table 1). The As−Mn distance of 3.13 Å is similar to that observed (3.16 Å) by Foster et al. (*32*), which was attributed to a bidentate−binuclear complex with δ-MnO_2. However, the observed 3.13 Å As−Mn distance is shorter than the ~3.22 Å As−Mn distance attributed to a bidentate−binuclear complex by both Manceau et al. (*31*) and Manning et al. (*14*). Quantum chemical calculations of As^{V} sorption in a bidentate−binuclear complex on Mn^{IV} also predict an As^{V}−Mn^{IV} distance of 3.20 Å (*23*). One possible explanation for the longer As−Mn distances observed by Manceau (*31*) and Manning (*14*) could be the presence of Mn^{III} on the surface (i.e., at edge sites) of the Mn-oxides used in these studies. Mn^{III} octahedra undergo Jahn−Teller distortion that is exhibited in a lengthening of two of the six Mn−O bonds in the octahedra. If some As^{V} is bound to Mn^{III} on the mineral surfaces used by Manceau et al. (*31*) and Manning et al. (*14*), it is reasonable to assume the resulting As−Mn distance would increase. We can reasonably describe the 3.13 Å As−Mn distance observed here as representing a bidentate−binuclear complex between As^{V} and δ-MnO_2.

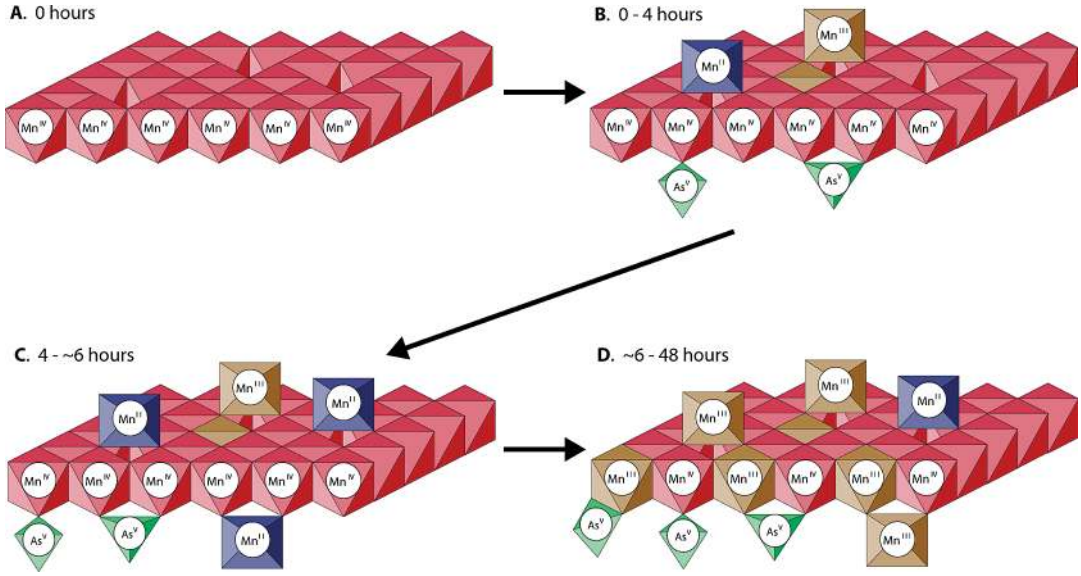

FIGURE 4. Proposed reaction mechanism for As^{III} oxidation by δ-MnO_2 over 48 h in a stirred-flow reactor. Throughout the reaction, As^{III} is oxidized by Mn^{IV} at δ-MnO_2 edge sites, producing Mn^{II} and As^{V}. (A) Unreacted δ-MnO_2 octahedral layers consist of primarily Mn^{4+} and have reaction sites at layer edges (edge sites) and vacancy sites. (B) During the first 4 h of As^{III} oxidation, Mn^{II} sorbs at δ-MnO_2 vacancy sites, and As^{V} sorbs at edge sites in bidentate−binuclear and monodentate−mononuclear complexes. Also, a portion of sorbed Mn^{II} reacts with Mn^{IV} at vacancy sites to form Mn^{III}. (C) Between 4 and ~6 h of reaction, vacancy sites become filled with $Mn^{II/III}$, Mn^{II} begins to sorb at δ-MnO_2 edge sites, and As^{V} sorption continues in the same sorption complexes. (D) Beyond ~6 h of reaction, Mn^{II} at edge sites (and probably vacancy sites) reacts with Mn^{III} in δ-MnO_2 octahedral layers to form Mn^{III}. The resulting Mn^{III} changes the bonding environment of As^{V}, which begins to sorb in bidentate−mononuclear complexes, and the As−Mn distance in As^{V} bidentate−binuclear complexes increases slightly.

A second As−Mn distance of 3.48 Å is also present when As^{V} is reacted with δ-MnO_2 (Table 1). An As−Mn distance similar to this has not been previously observed for As^{V} bound to Mn-oxides. However, Foster et al. (*32*) modeled As^{V} sorption on δ-MnO_2 in a monodentate−mononuclear complex and predicted an As−Mn distance of 3.6 Å, similar to the As^{V}−Fe distance observed for the same type of complex (*38, 39*). The Fe−O distance in an Fe octahedra (*39*) is 2.1 Å, while the Mn−O distance in Mn octahedra in this study are 1.9 Å (Table S1). Taking this difference into account, it is reasonable to conclude that the As−Mn distance of 3.48 Å observed in the As^{V} sorption standard represents a monodentate−mononuclear sorption complex between As^{V} and the δ-MnO_2 surface.

When As^{III} is reacted with δ-MnO_2, As^{V} is present on the δ-MnO_2 surface in the same sorption complexes (bidentate−binuclear and monodentate−mononuclear) for the first 4 h, as when As^{V} is sorbed on δ-MnO_2 (Table 1, Figure 4b). One can clearly see in the Fourier transformed data (Figure 3C) that As^{V} sorbed on δ-MnO_2, and the samples representing 0.5 and 4 h of reaction between As^{III} and δ-MnO_2, differ from 10, 24, and 48 h samples in the 2.2 and 3.2 Å region ($R + \Delta R$). However, the Fourier transformed data obtained after 10, 24, and 48 h are quite similar (Figure 3). Also, the monodentate−mononuclear complex between As^{V} and the δ-MnO_2 surface is present when As^{V} is sorbed as well as throughout As^{III} oxidation with a relatively consistent As−Mn distance (Table 1).

A change in As bonding environment on the δ-MnO_2 surface occurs between 4 and 10 h of reaction. This change occurs simultaneously with maximum Mn sorption at vacancy sites and the greatest Mn^{III} increase in the δ-MnO_2 structure (Figure 4c and 4d). From 10 to 48 h, an As−Mn distance of 2.7 Å appears, which corresponds to a bidentate−mononuclear (edge-sharing) complex between As^{V} and the δ-MnO_2 surface. The same complex observed on Fe-oxides is characterized by a Fe−O distance of 2.85 Å (*38*), which is longer than in this study, possibly due to the larger size of Fe^{III} octahedra compared to Mn^{IV} octahedra. However, an As−Mn distance of 2.7 Å can be reproduced by sorbing As^{V} on γ-$Mn^{III}OOH$ (Table 1), which might indicate that the bidentate−mononuclear complex observed during As^{III} oxidation by δ-MnO_2 is caused by As^{V} binding to Mn^{III} on the δ-MnO_2 surface rather than Mn^{IV} (Figure 4d).

Also observed between 4 and 10 h of reaction is a lengthening of the As−Mn distance attributed to a bidentate−binuclear complex from 3.13 Å to 3.21 Å (Table 1). This longer As−Mn distance (3.21 Å) is similar to the distances attributed to As bidentate−binuclear complexes on other phyllomanganates (*14, 31*). In our system it is possible that the increased As−Mn distance from 3.13 Å to 3.21 Å is due to As being bound, in part, to Mn^{III} rather than Mn^{IV} on the δ-MnO_2 surface (Figure 4d). This seems likely since the change in the As−Mn distance associated with bidentate−binuclear adsorption complexes coincides with the greatest increase in Mn^{III} on the δ-MnO_2 surface as discussed previously. Figure 4d includes a schematic representation of all observed As^{V} sorption complexes on the δ-MnO_2 surface.

Although, in this study, As^{III} oxidation probably does not directly form Mn^{III} on the δ-MnO_2 surface, it seems that the presence of Mn^{III} on a Mn-oxide surface can significantly alter the As local bonding environment. It also appears that Mn^{II} produced via reductive dissolution of δ-MnO_2 can passivate the δ-MnO_2 surface via sorption as well as comproportionation with Mn^{IV} to form Mn^{III} in the mineral structure. Passivation could be an important process in the environment because of its potential to decrease the sorption and oxidative capacities of some of the most reactive minerals in nature.

Acknowledgments

The authors thank three anonymous reviewers for their insightful comments, which strengthened this manuscript. The authors also thank Gerald Hendricks and Caroline Golt for laboratory assistance. B.L. is grateful for funding provided by a University of Delaware graduate fellowship and the Donald L. and Joy G. Sparks Graduate Fellowship in Soil Science. This research was funded by United States Depart-

ment of Agriculture Grant 2005-35107-16105, National Science Foundation Grant EAR-0544246, and Delaware National Science Foundation EPSCoR Grant EPS-0447610. Portions of this research were carried out at the SSRL, a national user facility operated by Stanford University on behalf of the U.S. Department of Energy, Office of Basic Energy Sciences. The SSRL Structural Molecular Biology Program is supported by the Department of Energy, Office of Biological and Environmental Research and by the National Institutes of Health, National Center for Research Resources, Biomedical Technology Program.

Supporting Information Available

Detailed solid-phase characterization methods, solid-phase sampling times, Mn XANES data, Mn XANES and EXAFS fitting results, and TEM images. This material is available free of charge via the Internet at http://pubs.acs.org.

Literature Cited

(1) Post, J. E. Manganese oxide minerals: Crystal structures and economic and environmental significance. *Proc. Natl. Acad. Sci. U.S.A.* **1999**, *96* (7), 3447–3454.
(2) Tebo, B. M.; Bargar, J. R.; Clement, B. G.; Dick, G. J.; Murray, K. J.; Parker, D.; Verity, R.; Webb, S. M. Biogenic manganese oxides: Properties and mechanisms of formation. *Annu. Rev. Earth Planet. Sci.* **2004**, *32*, 287–328.
(3) Villalobos, M.; Toner, B.; Bargar, J.; Sposito, G. Characterization of the manganese oxide produced by *Pseudomonas putida* strain MnB1. *Geochim. Cosmochim. Acta* **2003**, *67* (14), 2649–2662.
(4) Villalobos, M.; Lanson, B.; Manceau, A.; Toner, B.; Sposito, G. Structural model for the biogenic Mn oxide produced by Pseudomonas putida. *Am. Mineral.* **2006**, *91* (4), 489–502.
(5) Webb, S. M.; Tebo, B. M.; Bargar, J. R. Structural characterization of biogenic Mn oxides produced in seawater by the marine bacillus sp. strain SG-1. *Am. Mineral.* **2005**, *90* (8−9), 1342–1357.
(6) Toner, B.; Manceau, A.; Webb, S. M.; Sposito, G. Zinc sorption to biogenic hexagonal-birnessite particles within a hydrated bacterial biofilm. *Geochim. Cosmochim. Acta* **2006**, *70* (1), 27–43.
(7) Zhu, M.; Ginder-Vogel, M.; Sparks, D. L. Ni(II) sorption on biogenic Mn-oxides with varying Mn octahedral layer structure. *Environ. Sci. Technol.* **2010**, *44* (12), 4472–4478.
(8) Petrick, J. S.; Ayala-Fierro, F.; Cullen, W. R.; Carter, D. E.; Aposthian, H. V. Monomethylarsonous acid (MMA(III)) is more toxic than arsenite in Chang human hepatocytes. *Toxicol. Appl. Pharmacol.* **2000**, *163*, 203–207.
(9) Raven, K. P.; Jain, A.; Loeppert, R. H. Arsenite and arsenate adsorption on ferrihydrite: kinetics, equilibrium, and adsorption envelopes. *Environ. Sci. Technol.* **1998**, *32* (3), 344–349.
(10) Dixit, S.; Hering, J. G. Comparison of arsenic(V) and arsenic(III) sorption onto iron oxide minerals: Implications for arsenic mobility. *Environ. Sci. Technol.* **2003**, *37* (18), 4182–4189.
(11) Tournassat, C.; Charlet, L.; Bosbach, D.; Manceau, A. Arsenic(III) oxidation by birnessite and precipitation of manganese(II) arsenate. *Environ. Sci. Technol.* **2002**, *36* (3), 493–500.
(12) Moore, J. N.; Walker, J. R.; Hayes, T. H. Reaction scheme for the oxidation of As(III) to As(V) by birnessite. *Clays Clay Miner.* **1990**, *38* (5), 549–555.
(13) Chiu, V. Q.; Hering, J. G. Arsenic adsorption and oxidation at Manganite surfaces. 1. Method for simultaneous determination of adsorbed and dissolved arsenic species. *Environ. Sci. Technol.* **2000**, *34* (10), 2029–2034.
(14) Manning, B. A.; Fendorf, S. E.; Bostick, B.; Suarez, D. L. Arsenic(III) oxidation and arsenic(V) adsorption reactions on synthetic birnessite. *Environ. Sci. Technol.* **2002**, *36* (5), 976–981.
(15) Scott, M. J.; Morgan, J. J. Reactions at oxide surfaces. 1. Oxidation of As(III) by synthetic birnessite. *Environ. Sci. Technol.* **1995**, *29*, 1898–1905.
(16) Ginder-Vogel, M.; Landrot, G.; Fischel, J. S.; Sparks, D. L. Quantification of rapid environmental redox processes with quick-scanning x-ray absorption spectroscopy (Q-XAS). *Proc. Natl. Acad. Sci. U.S.A.* **2009**, *106*, 16124–16128.
(17) Parikh, S. J.; Lafferty, B. J.; Sparks, D. L. An ATR-FTIR spectroscopic approach for measuring rapid kinetics at the mineral/water interface. *J. Colloid Interface Sci.* **2008**, *320* (1), 177.
(18) Lafferty, B. J.; Ginder-Vogel, M.; Zhu, M.; Sparks, D. L. Arsenite oxidation by a poorly crystalline manganese oxide. 1. Stirred-flow experiments. *Environ. Sci. Technol.* **2010**, in press.
(19) Oscarson, D. W.; Huang, P. M.; Liaw, W. K.; Hammer, U. T. Kinetics of oxidation of arsenite by various manganese dioxides. *Soil Sci. Soc. Am. J.* **1983**, *47* (4), 644–648.
(20) Nesbitt, H. W.; Canning, G. W.; Bancroft, G. M. XPS study of reductive dissolution of 7 angstrom-birnessite by H_3AsO_3, with constraints on reaction mechanism. *Geochim. Cosmochim. Acta* **1998**, *62* (12), 2097–2110.
(21) Oscarson, D. W.; Huang, P. M.; Liaw, W. K. Role of manganese in the oxidation of arsenite by freshwater sediments. *Clays Clay Miner.* **1981**, *29*, 219–225.
(22) Tani, Y.; Miyata, N.; Ohashi, M.; Ohnuki, T.; Seyama, H.; Iwahori, K.; Soma, M. Interaction of inorganic arsenic with biogenic manganese oxide produced by a Mn-oxidizing fungus, strain KR21-2. *Environ. Sci. Technol.* **2004**, *38* (24), 6618–6624.
(23) Zhu, M.; Paul, K. W.; Kubicki, J. D.; Sparks, D. L., III. V) adsorption on Mn-oxides: Implications for arsenic(III) oxidation. *Environ. Sci. Technol.* **2009**, *43* (17), 6655–6661.
(24) Marcus, M. A.; Manceau, A.; Kersten, M. Mn, Fe, Zn and As speciation in a fast-growing ferromanganese marine nodule. *Geochim. Cosmochim. Acta* **2004**, *68* (14), 3125–3136.
(25) Drits, V. A.; Lanson, B.; Gaillot, A. C. Birnessite polytype systematics and identification by powder X-ray diffraction. *Am. Mineral.* **2007**, *92* (5−6), 771–788.
(26) Manceau, A.; Tommaseo, C.; Rihs, S.; Geoffroy, N.; Chateigner, D.; Schlegel, M.; Tisserand, D.; Marcus, M. A.; Tamura, N.; Chen, Z.-S. Natural speciation of Mn, Ni, and Zn at the micrometer scale in a clayey paddy soil using X-ray fluorescence, absorption, and diffraction. *Geochim. Cosmochim. Acta* **2005**, *69* (16), 4007–4034.
(27) Manceau, A.; Marcus, M. A.; Tamura, N.; Proux, O.; Geoffroy, N.; Lanson, B. Natural speciation of Zn at the micrometer scale in a clayey soil using X-ray fluorescence, absorption, and diffraction. *Geochim. Cosmochim. Acta* **2004**, *68* (11), 2467–2483.
(28) Silvester, E.; Manceau, A.; Drits, V. A. Structure of synthetic monoclinic Na-rich birnessite and hexagonal birnessite. 2. Results from chemical studies and EXAFS spectroscopy. *Am. Mineral.* **1997**, *82* (9−10), 962–978.
(29) Manceau, A.; Lanson, B.; Drits, V. A., III. Results from powder and polarized extended X-ray absorption fine structure spectroscopy. *Geochim. Cosmochim. Acta* **2002**, *66* (15), 2639–2663.
(30) Drits, V. A.; Silvester, E.; Gorshkov, A. I.; Manceau, A. Structure of synthetic monoclinic Na-rich birnessite and hexagonal birnessite. 1. Results from X-ray diffraction and selected-area electron diffraction. *Am. Mineral.* **1997**, *82* (9−10), 946–961.
(31) Manceau, A.; Lanson, M.; Geoffroy, N. Natural speciation of Ni, Zn, Ba, and As in ferromanganese coatings on quartz using X-ray fluorescence, absorption, and diffraction. *Geochim. Cosmochim. Acta* **2007**, *71* (1), 95–128.
(32) Foster, A. L.; Brown, G. E.; Parks, G. A. X-ray absorption fine structure study of As(V) and Se(IV) sorption complexes on hydrous Mn oxides. *Geochim. Cosmochim. Ac.* **2003**, *67* (11), 1937–1953.
(33) Villalobos, M.; Bargar, J.; Sposito, G. Mechanisms of Pb(II) sorption on a biogenic manganese oxide. *Environ. Sci. Technol.* **2005**, *39* (2), 569–576.
(34) Gaillot, A. C.; Flot, D.; Drits, V. A.; Manceau, A.; Burghammer, M.; Lanson, B. Structure of synthetic K-rich birnessite obtained by high-temperature decomposition of $KMnO_4$. I. Two-layer polytype from 800 °C experiment. *Chem. Mater.* **2003**, *15* (24), 4666–4678.
(35) Manceau, A.; Drits, V. A.; Silvester, E.; Bartoli, C.; Lanson, B. Structural mechanism of Co^{2+} oxidation by the phyllomanganate buserite. *Am. Mineral.* **1997**, *82* (11−12), 1150–1175.
(36) Zhu, M.; Ginder-Vogel, M.; Parikh, S. J.; Feng, X.-H.; Sparks, D. L. Cation effects on the layer structure of biogenic Mn-oxides. *Environ. Sci. Technol.* **2010**, *44* (12), 4465–4471.
(37) Webb, S. M.; Dick, G. J.; Bargar, J. R.; Tebo, B. M. Evidence for the presence of Mn(III) intermediates in the bacterial oxidation of Mn(II). *Proc. Natl. Acad. Sci. U.S.A.* **2005**, *102* (15), 5558–5563.
(38) Fendorf, S.; Eick, M. J.; Grossl, P. Arsenate and chromate retention mechanisms on goethite. 1. Surface structure. *Environ. Sci. Technol.* **1997**, *31*, 315–320.
(39) Waychunas, G. A.; Rea, B. A.; Fuller, C. C.; Davis, J. A. Surface chemistry of ferrihydrite, Part l. EXAFS studies of the geometry of coprecipitated and adsorbed arsenate. *Geochim. Cosmochim. Acta* **1993**, *57* (10), 2251–69.

ES102016C